



AD-A237 428



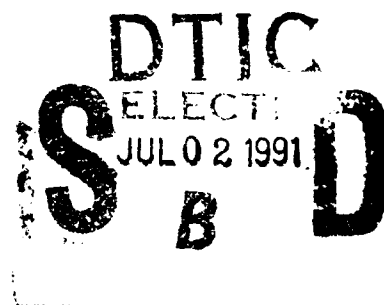
NRL Memorandum Report 6772

Vlasov Simulations of Very-Large-Amplitude Wave Generation in the Plasma Wakefield Accelerator

JONATHAN KRALL, GLENN JOYCE AND ERIC ESAREY

*Beam Physics Branch
Plasma Physics Division*

June 17, 1991



91-03581



REPORT DOCUMENTATION PAGE			Form Approved OMB No. 0704-0188	
<small>Public reporting burden for this collection of information is estimated to average 1 hour per response, including the time for reviewing instructions, searching existing data sources, gathering and maintaining the data needed, and completing and reviewing the collection of information. Send comments regarding this burden estimate or any other aspect of this collection of information, including suggestions for reducing this burden, to Washington Headquarters Services, Directorate for Information Operations and Reports, 1215 Jefferson Davis Highway, Suite 1204, Arlington, VA 22202-4302, and to the Office of Management and Budget, Paperwork Reduction Project (0704-0188), Washington, DC 20503.</small>				
1. AGENCY USE ONLY (Leave blank)		2. REPORT DATE 1991 June 17		3. REPORT TYPE AND DATES COVERED Interim
4. TITLE AND SUBTITLE Vlasov Simulations of Very-Large-Amplitude Wave Generation in the Plasma Wakefield Accelerator			5. FUNDING NUMBERS DE-AI05-83ER-40017	
6. AUTHOR(S) Jonathan Krall, Glenn Joyce and Eric Esarey				
7. PERFORMING ORGANIZATION NAME(S) AND ADDRESS(ES) Naval Research Laboratory Washington, DC 20375-5000			8. PERFORMING ORGANIZATION REPORT NUMBER NRL Memorandum Report 6772	
9. SPONSORING / MONITORING AGENCY NAME(S) AND ADDRESS(ES) DOE Washington, DC			10. SPONSORING / MONITORING AGENCY REPORT NUMBER	
11. SUPPLEMENTARY NOTES				
12a. DISTRIBUTION / AVAILABILITY STATEMENT Approved for public release; distribution unlimited.			12b. DISTRIBUTION CODE	
13. ABSTRACT (Maximum 200 words) Simulations of the plasma wakefield accelerator are carried out by following the time evolution of the plasma distribution function in one dimension via the Vlasov-Maxwell equations. Simulation results are compared to numerical solutions of the nonlinear relativistic cold plasma equations and to previous theoretical estimations of trapping and thermal effects on plasma waves. It is found that highly nonlinear wakes are obtainable in the vicinity of the driving beam, where the thermal velocity spread of the plasma is reduced. In this region, wake amplitudes can significantly exceed the expectations of relativistic warm plasma models and agree closely with cold fluid theory. In all cases, however, particle trapping and thermalization due to particle scattering from the large amplitude plasma wave reduce the wake to below the nonrelativistic wavebreaking limit after the initial accelerating peak.				
14. SUBJECT TERMS Nonlinear plasma waves Plasma wakefield accelerator Beam-plasma interactions			15. NUMBER OF PAGES 32	
			16. PRICE CODE	
17. SECURITY CLASSIFICATION OF REPORT UNCLASSIFIED	18. SECURITY CLASSIFICATION OF THIS PAGE UNCLASSIFIED	19. SECURITY CLASSIFICATION OF ABSTRACT UNCLASSIFIED	20. LIMITATION OF ABSTRACT SAR	

CONTENTS

I. INTRODUCTION.....	1
II. 1D NONLINEAR VLASOV FORMULATION.....	4
III. SIMULATIONS IN THE LINEAR REGIME.....	7
IV. SIMULATIONS IN THE NONLINEAR REGIME.....	9
V. NONLINEAR PLASMA WAKEFIELD ACCELERATOR.....	12
VI. CONCLUSIONS.....	14
ACKNOWLEDGMENTS.....	15
APPENDIX: VLASOV-MAXWELL SIMULATIONS IN ONE DIMENSION.....	16
REFERENCES.....	19
TABLE I.....	21



Accession For	
NTIS GRA&I	<input checked="" type="checkbox"/>
DTIC TAB	<input type="checkbox"/>
Unannounced	<input type="checkbox"/>
Justification	
By	
Distribution/	
Availability Codes	
Dist	Avail and/or Special
A-1	

VLASOV SIMULATIONS OF VERY-LARGE-AMPLITUDE WAVE GENERATION IN THE PLASMA WAKEFIELD ACCELERATOR

I. INTRODUCTION

Novel plasma-based acceleration devices¹⁻³ are being actively researched due to their ability to support acceleration gradients in excess of 10 GeV/m, which is greater than two orders of magnitude beyond those obtainable in conventional linear accelerators. The plasma wakefield accelerator (PWFA)² is one such device, wherein a moderate-energy electron beam drives a plasma wave which, in turn, accelerates a high-energy electron bunch. This process has been demonstrated experimentally.⁴ Of interest in this scheme are limits on the obtainable accelerating gradients and transformer ratios in the plasma wakefield.

The transformer ratio is defined as

$$R \equiv E_+ / E_- \quad (1)$$

where E_- is the peak decelerating field experienced by the driving electron beam and E_+ is the peak accelerating field in the wake. The physical significance of the transformer ratio is that the energy gained by the trailing beam in a single acceleration stage, ΔW , is given approximately by $\Delta W = RW_0$, where W_0 is the energy of the driving beam. Theoretical results for linear wakefields have suggested that driving beam pulses that are symmetric in the axial dimension produce transformer ratios that are limited to $R \leq 2$.⁵ Further results showed that higher transformer ratios may be obtained by using a nonsymmetric beam pulse⁶ or by operating in the nonlinear regime.⁷ The difficulties associated with generating a shaped beam pulse add to the attractiveness of the nonlinear PWFA approach. The viability of the nonlinear PWFA, however, may be limited by the effects of plasma temperature and trapping of plasma electrons by the large amplitude

wave. For the present study we will consider, via simulation, generation of nonlinear plasma waves by a symmetric beam pulse.

The properties of large-amplitude waves in cold plasmas have been studied by a number of researchers.^{2,7-12} For nonrelativistic plasma waves, it was found that the peak electric field was limited by the nonrelativistic wave-breaking field:⁹

$$E_{\max} = mv_{\text{ph}}\omega_p/e < E_{\text{wb}} = mc\omega_p/e \quad (2)$$

where m is the electron mass, v_{ph} is the phase velocity of the plasma wave, e , assumed positive, is the elementary charge, c is the speed of light in vacuum, $\omega_p = (4\pi n_0 e^2/m)^{1/2}$, and n_0 is the equilibrium plasma density. As v_{ph} approaches c , $E_{\max} \approx E_{\text{wb}}$. Note, for instance, that at $n_p = 10^{14} \text{ cm}^{-3}$, $E_{\text{wb}} = 1 \text{ GeV/m}$. Coffey¹³, using the nonrelativistic Vlasov-Poisson equations and a "waterbag" distribution function for the plasma electrons, showed that this amplitude is reduced for a warm plasma. In this case,

$$E_{\max} = (mv_{\text{ph}}\omega_p/e)(1 - \frac{1}{3}\mu - \frac{8}{3}\mu^{1/4} + 2\mu^{1/2})^{1/2}, \quad (3)$$

where $\mu = 3T/mv_{\text{ph}}^2$ and T is the plasma thermal energy.

For relativistic plasma waves, $E > E_{\text{wb}}$ is possible. For a cold plasma, the limit is⁸

$$E_{\max} = (mc\omega_p/e)\sqrt{2}(\gamma_{\text{ph}} - 1)^{1/2}, \quad (4)$$

where $\gamma_{\text{ph}} = (1 - v_{\text{ph}}^2/c^2)^{-1/2}$. This suggests that as v_{ph} approaches c , $E \gg E_{\text{wb}}$ is possible. As in the nonrelativistic case, this limit is reduced by thermal effects. Katsoulas and Mori¹⁴ performed a calculation similar to

that of Ref. 13 for the relativistic case. Again a waterbag distribution function was used. They found

$$E_{\max} = (mc\omega_p/e)\mu^{-1/4}[\ln(2\gamma_{ph}^{1/2}\mu^{1/4})]^{1/2}, \quad (5)$$

which is assumed to be valid as long as it gives a smaller value than Eq. (4), as is the case for parameters of interest. An alternative approach was taken by Rosenzweig¹⁵, who calculated the saturation amplitude of the plasma wave in two ways. Firstly, from an energy balance argument involving loading due to the trapped portion of a Gaussian velocity distribution, he found:

$$E_{\max} \approx (mc\omega_p/e)(mc^2/4T)^{1/4}. \quad (6)$$

Secondly, from a warm fluid plasma model, he found a similar expression:

$$E_{\max} \approx (mc\omega_p/e)(4mc^2/27T)^{1/4}. \quad (7)$$

In Eqs. (6) and (7) it was assumed that $v_{ph} = v_b$, where v_b is the velocity of the driving beam, $\gamma_b = (1 - v_b^2/c^2)^{-1/2} \gg 1$ and $\gamma_b \gg 1/\mu$. These approximate expressions are interesting in that they are (approximately) independent of γ_{ph} . In a later calculation, employing a three-fluid model for the thermal plasma, Rosenzweig found¹⁶

$$E_{\max} \approx (mc\omega_p/e)(\gamma_b mc^2/27T)^{1/4}, \quad (8)$$

which gives results that are similar to those of Eq. (5) for parameters of interest here. This is not surprising in that, with both the three-fluid and the waterbag models, there are no plasma electrons with $p > p_{crit}$,

where p_{crit} is the thermal momentum in the three-fluid model and the surface momentum of the waterbag in the waterbag model. In either case, the onset of trapping is quite sudden.

In this paper we present simulations of plasma waves driven by a non-relativistic electron beam with velocity v_b . These are carried out by following the time evolution of the plasma distribution function in one spatial dimension via the Vlasov-Maxwell equations. Direct simulation via the Vlasov equation is an ideal way of examining thermal and trapping effects because the artificially high temperatures associated with typical particle simulations are avoided.

In following sections we first describe the Vlasov-Maxwell equations for this system. We include a discussion of the cold plasma equations to which we will compare our results. We then present simulations in the linear and nonlinear cases, including simulations of the so-called nonlinear PWFA⁷ in which a plasma wave is driven by a beam of length $L_b/\lambda_p \gg 1$, where $\lambda_p = 2\pi v_{ph}/\omega_p$, to provide $R \gg 1$ and $E_+/E_{wb} \gg 1$.

II. 1D NONLINEAR VLASOV FORMULATION

To simulate plasma wave generation we use the Vlasov-Maxwell equations:

$$\frac{\partial f}{\partial t} + \frac{p_z}{\gamma m} \frac{\partial f}{\partial z} + eE_z \frac{\partial f}{\partial p_z} = 0 \quad (9)$$

and

$$\frac{\partial E_z}{\partial z} = -4\pi e(n + n_b - n_0) , \quad (10)$$

where $f(z, p_z, t)$ is the distribution function, $\gamma = (1 + p_z^2/m^2 c^2)^{1/2}$, n_b is the driving beam density, E_z is the electric field and

$$n = \int dp_z f . \quad (11)$$

For this system, Maxwell's equations reduce simply to Gauss's law. Changing variables from (z, p_z, t) to $(\zeta = ct - z, p_z, \tau = t)$, we have

$$\frac{\partial f}{\partial \tau} + (c - \frac{p_z}{\gamma m}) \frac{\partial f}{\partial \zeta} + e E_z \frac{\partial f}{\partial p_z} = 0 , \quad (12)$$

and

$$\frac{\partial E_z}{\partial \zeta} = 4\pi e(n + n_b - n_0) . \quad (13)$$

The simulation is carried out by solving for $E_z(\zeta, \tau)$ from the current value of $f(\zeta, p_z, \tau)$ via Eqs. (11) and (13) and subsequently updating f via Eq. (12). Initially f is uniform in z and Gaussian in p_z , varying as $\exp(-p_z^2/2mT_0)$, where T_0 is the equilibrium plasma thermal energy. We represent the driving beam as a fixed charge shape that propagates with velocity v_b but that otherwise does not evolve. The details of the simulation code are discussed in the appendix.

For comparison to our simulation results, we consider the cold-fluid limit of the Vlasov equation, which we discuss here. For a non-evolving electron beam with $v_b \approx c$, steady-state may be assumed and derivatives with respect to τ may be neglected. It is convenient to work in terms of the normalized scalar potential, $\phi = e\Phi/mc^2$, the normalized electron velocity, $\beta_z = v_z/c$, and the normalized electron momentum, $u_z = \gamma\beta_z$, where $\gamma =$

$(1+u_z^2)^{1/2}$. In these variables, the relativistic Vlasov equation (12) becomes

$$\left[(1 - \beta_z) \frac{\partial}{\partial \zeta} - \left(\frac{\partial \phi}{\partial \zeta} \right) \frac{\partial}{\partial u_z} \right] f = 0 , \quad (14)$$

where $f = f(\zeta, u_z)$.

Analysis of the characteristics of the above equation indicate that there exists a constant of the motion, $w = \gamma - u_z - \phi$, which is the normalized electron energy in wakefield frame. Hence, any distribution which is a function of this constant of the motion,

$$f(w) = f(\gamma - u_z - \phi) , \quad (15)$$

is a general nonlinear solution of the relativistic Vlasov equation. In terms of the normalized momentum u_z , the distribution $f(w)$ is related to $f(u_z)$ by $du_z f(u_z) = dw f(w) |du_z/dw|$, where $|du_z/dw| = [1 + (w+\phi)^{-2}]^{1/2}$.

We now consider the cold plasma limit. This limit is valid as long as the thermal velocity is small compared to the trapping width of the plasma wave, $v_{th} \ll |v_p - \bar{v}_z|$, where \bar{v}_z is the bulk longitudinal motion of the electrons in the plasma wave. This inequality holds for plasma wave amplitudes sufficiently below wavebreaking. The cold plasma electron distribution function is given by $f(w) \approx n_0 \delta(w - 1)$, i.e.,

$$f(w) = n_0 \delta(\gamma - u_z - \phi - 1) , \quad (16)$$

where n_0 is the ambient plasma electron density. Analytically, thermal effects may be included by choosing a more appropriate distribution function $f(w)$, such as a waterbag or a Gaussian distribution.¹⁷

Using Eq. (16), various moments may be calculated, i.e., the electron fluid density $n(\zeta) = \int du_z f(u_z)$ and the electron fluid velocity $\bar{\beta}_z = n^{-1} \int du_z (u_z/\gamma) f(u_z)$. One finds

$$n = n_0 [1 + (1 + \phi)^{-2}] / 2 \quad (17)$$

and

$$\bar{\beta}_z = [1 - (1 + \phi)^2] / [1 + (1 + \phi)^2] . \quad (18)$$

Using Poisson's equation, the self-consistent nonlinear equation describing $\phi(\zeta)$ is

$$\frac{d^2 \phi}{d\zeta^2} = \frac{k_p^2}{2} [2n_b/n_0 + (1 + \phi)^{-2} - 1] , \quad (19)$$

where $k_p = \omega_p/c$. Equation (19) describes the generation of nonlinear wakefields in a cold plasma by a non-evolving beam $n_b(\zeta)$ with $v_b \approx c$. A similar equation may be derived to describe the generation of nonlinear wakefields by an intense laser pulse.¹²

The cold plasma equations, Eqs. (17)-(19), were previously derived by Rosenzweig^{7,15} using cold fluid theory and were subsequently used to analyze plasma wakefield generation. Numerical solutions to Eqs. (17)-(19) will be compared to the simulations discussed below.

III. SIMULATIONS IN THE LINEAR REGIME

Simulations in the linear regime showed excellent agreement with theory for $T_0 \leq 5$ keV. Here, we considered $n_0 = 2 \times 10^{14} \text{ cm}^{-3}$, such that

$\lambda_p = 2\pi c/\omega_p = 0.236$ cm and $E_{wb} = 1.36$ GeV/m. The driving beam was of the form

$$n_b = \begin{cases} n_{b0} \sin\{\pi[\zeta - (c-v_b)\tau]/L_b\} & (c-v_b)\tau \leq \zeta \leq (c-v_b)\tau + L_b \\ 0 & \text{otherwise} \end{cases} \quad (20)$$

with $n_{b0}/n_0 = 0.1$, $L_b = 0.24$ cm $\approx \lambda_p$ and $\gamma_b = 100$. For these runs, we modelled a region of phase space bounded by $0 \leq \zeta \leq 1.024$ cm and $-10.2 \leq p_z/mc \leq 30.7$ with simulation parameters $\Delta\zeta = 10^{-3}$ cm and $\Delta p_z/mc = 4 \times 10^{-2}$. After 1.6 cm of propagation, a near-steady state was established.

Subsequent runs at $T_0 = 19$ keV showed deviations of $\approx 5\%$ from the cold plasma equations. These were consistent with warm fluid calculations. For instance, Ref. 14 points out that the warm-fluid oscillation wavelength is

$$\lambda = \lambda_p (v_{ph}/c) [1 - \frac{3}{2}(v_{th}/v_{ph})^2]^{1/2} \quad (21)$$

in agreement with our results, assuming $v_{ph} = v_b$.

We diagnosed the plasma temperature as

$$T = P/n \quad (22)$$

with P given by¹⁸

$$P = \int dp_z (p_z - \bar{p}_z)(v_z - \bar{v}_z) f \quad (23)$$

where \bar{p}_z and \bar{v}_z are the average momentum and velocity as given by moments $f(z, p_z, \tau)$. In the linear runs, T increased over the several plasma wavelengths of the simulation region but with minimal impact on the results.

IV. SIMULATIONS IN THE NONLINEAR REGIME

A series of simulations were performed with the beam profile given in Eq. (20) with $n_{b0}/n_0 = 0.1, 0.2, 0.3, 0.4$ and 0.5 , $L_b = 0.24 \text{ cm} \approx \lambda_p$, $\gamma_b = 100$ and $T_0 = 19 \text{ keV}$. Peak electric fields and corresponding theoretical values are plotted versus n_{b0}/n_0 in Fig. 1. Simulation parameters were as in the linear-regime runs. As an example, the beam density, electric field and perturbed plasma density, $n_1 = n - n_0$, are plotted in Fig. 2 for the $n_{b0}/n_0 = 0.5$ case. Figure 3 shows the corresponding results from the cold plasma equations. Note that in our plotting convention $E_z > 0$ is accelerating.

In the most highly nonlinear cases, $n_{b0}/n_0 = 0.4$ and 0.5 , several interesting phenomena were observed:

(1) Excellent agreement with the cold plasma equations was observed up to the first accelerating E_z peak. In this region the temperature, given by Eq. (22-23) and plotted in Fig. 4 for the $n_{b0}/n_0 = 0.5$ case, drops by an order of magnitude. Results did not vary when the initial plasma temperature was decreased to $T_0 = 5 \text{ keV}$ (see Fig. 4). For reasons of numerical expense, it is difficult to drop the temperature further in the code.

(2) Particle trapping was observed at the initial accelerating peak in E_z . This is shown in Fig. 5, where the plasma electron distribution is plotted versus p_z and ζ . Here, a small portion of the electron distribution was accelerated to the simulation boundary at $p_{z,\text{max}}/mc = 30.7$, where the boundary condition dictates $f=0$. The loss of plasma electrons at the $p_z = p_{z,\text{max}}$ boundary changed the results by <1% relative to a case in which $p_{z,\text{max}}/mc = 60.0$ was used. A later run with $p_{z,\text{max}}/mc = 5.12$ showed no change in either of the first two accelerating peaks in E_z .

This suggests that the trapped particle distribution is not a significant load on the wakefield.

(3) Relativistic lengthening of the wake was observed. This was not in agreement with Ref. 15, however, wherein $\lambda \approx 4\sqrt{2}\bar{\gamma}_m c/\omega_p$. The difficulty is that trapped and nearly-trapped particles increase $\bar{\gamma}_m$ beyond the expectations of the cold fluid model. Here, $\bar{\gamma}$ is the average value of γ as given by a moment of $f(\zeta, p_z, \tau)$.

(4) The wakefield, $E_z(\zeta)$, decreased after the first peak to a value less than the nonrelativistic wave-breaking limit of Eq. (2). This low value of E_z was accompanied by an increased plasma temperature. Again, this result did not vary with T_0 .

(5) Results were independent of γ_b for $\gamma_b \geq 10$. At $\gamma_b = 5$, a significant increase both in trapping and plasma heating was observed. Note that $\gamma_b = 5$ is highly unphysical, given our non-evolving beam.

Both the close agreement with the cold plasma equations in the region near the beam, where the wakefield is larger than might be expected for a $T \approx 19$ keV plasma, and the sudden thermalization behind the initial E_z peak, where the wakefield amplitude is somewhat reduced, are unexpected results.

The close agreement between the simulation and the cold plasma equations in the region near the beam may be explained by a simple argument. In the region near the beam, plasma electrons are accelerated in bulk in the direction opposite the phase velocity of the wave. This acceleration reduces the longitudinal thermal motion of the plasma electrons. The resulting cold plasma distribution closely reproduces the results of the cold plasma equations. From Eqs. (22-23),

$$T \sim P \sim \int dp_z f \Delta\gamma \left(\frac{1}{\gamma^2} - \frac{1}{\gamma^2} \right) \sim \frac{1}{\gamma^3} \quad (24)$$

where $\Delta\gamma = \gamma - \bar{\gamma}$ and we have assumed that $n(\zeta)$ is constant over the accelerating region and that $\gamma \gg 1$ and $\Delta\gamma \ll \gamma$ for regions in which $f > 0$. A similar relation between thermal velocity and $\bar{\gamma}$ has been observed in conventional induction accelerators.¹⁹ This effect will be evident in the highly nonlinear runs presented below.

The physics behind the initial peak in E_z , where thermalization of the plasma electrons is associated with a lower value of the wake amplitude, is less clear than the situation near the driving beam. Thermalization is apparently caused by scattering of the plasma electrons from the large amplitude plasma wave and may be associated with the fraction of plasma electrons that are nearly-trapped, remaining in the region of peak density for times of the order of ω_p^{-1} .

Evidence for this concept is provided by a run in which we set $\gamma_b = 5$. Lowering v_{ph} allowed a significant increase (relative to the $\gamma \geq 10$ cases) in the density of trapped and nearly-trapped electrons and an increase in the thermal energy in the wake by approximately a factor of two. Further evidence is provided in Fig. 4, wherein a lower value of T_0 increased (slightly) the thermal energy in the wake. We speculate that the lower T_0 provided a more coherent nonlinear oscillation and stronger scattering of the electron distribution. The temperature diagnostic is difficult to interpret, however, in that T is lowered in the decelerating phase of the plasma wave by the bulk acceleration mechanism described above. In the accelerating phase of the plasma wave, T is artificially increased by trapped and nearly-trapped electrons.

If we take $T = 50$ keV, we can somewhat explain the low value of E_z behind the first peak by the theoretical saturation limits given in Ref. 15 and quoted as Eqs. (6) and (7) above. These give $E_{\max}/E_{wb} = 1.26$ and 1.10

respectively. Equation (5) gives the much higher value of $E_{\max}/E_{wb} = 2.22$, suggesting that elements of the model of Ref. 15, particularly the trapping process, represent physics that comes into play before the limit of Ref. 14 is reached. It is interesting to note that our results are independent of γ_b for $\gamma_b \geq 10$ whereas Eqs. (4), (5) and (8) vary with γ_b . This suggests that expectations based on Eqs. (4), (5) and (8) may not be meaningful in this instance as long as one assumes $v_{ph} = v_b$.

V. NONLINEAR PLASMA WAKEFIELD ACCELERATOR

For a beam pulse with $n_b = n_p/2$ and $L_b > \lambda_p$, theory suggests that transformer ratios $R \gg 2$ may be obtained. We consider a beam pulse of the form:

$$n_b = \begin{cases} n_p/2 & (c-v_b)\tau \leq \zeta \leq (c-v_b)\tau + L_b \\ 0 & \text{otherwise} \end{cases} \quad (25)$$

The nonlinear cold plasma equations, (17)-(19), have been solved for this case.⁷ Defining $x \equiv (1 + \phi)$ and $\xi \equiv \omega_p(t - z/v_b)$, $x(\xi)$ within the beam is given implicitly by

$$\xi = x^{1/2}(x - 1)^{1/2} + \ln[(x - 1)^{1/2} + x^{1/2}] \quad (26)$$

Defining $\xi_f \equiv 2\pi L_b/\lambda_p$ and $x_f \equiv x(\xi_f)$, it can be shown that the maximum fields within and behind the beam, respectively, are given by

$$E_- = \frac{mc\omega}{e} (1 - 1/x_f)^{1/2} \quad (27)$$

and

$$E_+ = \frac{mc\omega}{e} p (x_f - 1)^{1/2} \quad (28)$$

such that the transformer ratio is

$$R = E_+/E_- = x_f^{1/2}. \quad (29)$$

Vlasov-Maxwell simulations of the nonlinear plasma wakefield accelerator were performed with parameters similar to those of the linear and nonlinear cases above: $n_p = 2 \times 10^{14} \text{ cm}^{-3}$, $T_0 = 19 \text{ keV}$, n_b given by Eq. (25) and $\gamma_b = 100$. In this case, however, we use $L_b/\lambda_p = 0.83, 1.63$ and 2.79 such that Eqs. (26-29) give $R = 2, 3$ and 4 respectively.

Simulation results are summarized in Table I. Cold plasma model results are also given. As an example, the beam density, electric field and perturbed plasma density, $n_1 = n - n_0$, are plotted in Fig. 6 for the $L_b/\lambda_p = 2.79$ case.

As before, we observe a reduction in the thermal velocity spread of the plasma in the region near the beam, excellent agreement with the cold plasma equations up to the initial accelerating peak, thermalization of the plasma behind the initial peak in E_z , and a drop in E_z to $E_z \leq E_{wb}$ thereafter. In the $L_b/\lambda_p = 2.79$ case, the temperature behind the initial E_z peak was diagnosed by smoothly setting $E_z = 0$ beyond this point and allowing the oscillating plasma to "settle". Results indicate $50 \text{ keV} < T < 150 \text{ keV}$.

Agreement with the cold plasma model up to the first peak is made clear when Fig. 6 is compared to Fig. 1 of Ref. 7. In fact, the $L_b/\lambda_p = 2.79$ case shows a peak electric field which, while down by 6% from the cold plasma result, exceeds the expectations of Eqs. (5-8) for a $T_0 = 19 \text{ keV}$

plasma. This surprising result is caused by the reduction in the thermal velocity spread in the plasma in accordance with Eq. (24) as is observed in Fig. 7, which shows plots of T and $\bar{\gamma}$ for this case.

Our observation of $E_z \lesssim E_{wb}$ following the initial E_z peak is interesting in light of Eqs. (2-8). Again we find relativistic oscillations of the hot plasma limited in a way most closely corresponding to Eqs. (6-7). Taking $T = 100$ keV after the first peak, Eqs. (6) and (7) give $E_{\max}/E_{wb} = 1.06$ and 0.93 respectively, in reasonable agreement with Figs. 6 and 7. As before, Eqs. (5) and (8) give higher values of E_{\max} .

VI. CONCLUSIONS

Simulations of the plasma wakefield accelerator were carried out by following the time evolution of the plasma distribution function in one dimension via the Vlasov-Maxwell equations. Results were in surprisingly good agreement with numerical solutions of the nonlinear relativistic cold plasma equations in the vicinity of the driving beam, where the thermal velocity spread of the plasma is reduced by the mechanism of Eq. (24). This reduction in the plasma thermal velocity allowed the generation of wake amplitudes that exceeded of the predictions of relativistic warm plasma models as given in Eqs. (5-8).

Thermalization of the plasma, however, apparently due to particle scattering from the large amplitude plasma wave, limited the wake to $E_z \lesssim E_{wb}$ behind the initial accelerating peak. The thermal energy in this region was observed to increase with the density of nearly-trapped particles (those that remain in the region of peak density for times of the order of ω_p^{-1}). Wake amplitude limits behind the initial accelerating peak

were in reasonable agreement with Ref. 15. This agreement may be serendipitous, however, given the complexity of the observed phenomena.

These results were insensitive to γ_b for $\gamma_b \geq 10$ and to the equilibrium plasma temperature over the range $3 \text{ keV} < T_0 < 20 \text{ keV}$. Results were also insensitive to the presence or removal of the trapped portion of the distribution function.

Finally, the nonlinear PWFA concept of Ref. 7 was found to be viable, within the context of the one-dimensional simulation, up to the first accelerating peak. Here, a transformer ratio $R = 3.78$ was demonstrated for a case in which the theoretical value was $R = 4$.

ACKNOWLEDGMENTS

The authors would like to thank J. Rosenzweig, T. Katsouleas and W. Mori for many useful and enlightening discussions. This work was supported by the U. S. Department of Energy and the Office of Naval Research.

APPENDIX: VLASOV-MAXWELL SIMULATIONS IN ONE DIMENSION

To model beam-plasma and laser-plasma interactions, we have developed numerical solutions of the relativistic Vlasov-Maxwell system of equations for implementation on the Connection Machine at the U. S. Naval Research Laboratory. For further numerical discussions of the relativistic Vlasov equation see Ref. 20.

The code is formulated in $(\zeta, p_x, p_y, p_z, \tau)$ coordinates where $\zeta = ct - z$ and $\tau = t$. The Vlasov equation in this case has only one spatial dimension:

$$\frac{\partial f}{\partial \tau} + (c - \frac{p_z}{\gamma m}) \frac{\partial f}{\partial \zeta} + \frac{\partial}{\partial p_z} [(E_z + \frac{p_x B_y}{\gamma m c} - \frac{p_y B_x}{\gamma m c}) f] = 0, \quad (A1)$$

where $f(\zeta, p_z, \tau)$ is a reduced distribution function for the plasma, p_x and p_y are momenta which are determined from canonical momentum conservation, $\gamma = [1 + (p_x^2 + p_y^2 + p_z^2)/m^2 c^2]^{1/2}$ and E_x, E_y, E_z, B_x and B_y are determined from Maxwell's equations.

Here, Maxwell's equations are formulated in the Lorentz gauge. In terms of the potentials, A_x, A_y and $\alpha = A_z - \Phi$,

$$\frac{1}{c} \frac{\partial^2 \alpha}{\partial \tau^2} + 2 \frac{\partial^2 \alpha}{\partial \zeta \partial \tau} = 4\pi(J_z - \rho c), \quad (A2)$$

$$\frac{1}{c} \frac{\partial^2 A_x}{\partial \tau^2} + 2 \frac{\partial^2 A_x}{\partial \zeta \partial \tau} = 4\pi J_x, \quad (A3)$$

$$\frac{1}{c} \frac{\partial^2 A_y}{\partial \tau^2} + 2 \frac{\partial^2 A_y}{\partial \zeta \partial \tau} = 4\pi J_y, \quad (A4)$$

and

$$\frac{1}{c} \frac{\partial^2 \Phi}{\partial \tau^2} + 2 \frac{\partial^2 \Phi}{\partial \zeta \partial \tau} = 4\pi\rho , \quad (\text{A5})$$

where \underline{J} and ρ are the current and charge densities, respectively. The fields are given by

$$E_z = -\frac{1}{c} \frac{\partial \alpha}{\partial \tau} - \frac{\partial \alpha}{\partial \zeta} - \frac{1}{c} \frac{\partial \Phi}{\partial \tau} , \quad (\text{A6})$$

$$E_x = -\frac{1}{c} \frac{\partial A_x}{\partial \tau} - \frac{\partial A_x}{\partial \zeta} , \quad (\text{A7})$$

$$E_y = -\frac{1}{c} \frac{\partial A_y}{\partial \tau} - \frac{\partial A_y}{\partial \zeta} , \quad (\text{A8})$$

$$B_x = \frac{\partial A_y}{\partial \zeta} , \quad (\text{A9})$$

and

$$B_y = -\frac{\partial A_x}{\partial \zeta} . \quad (\text{A10})$$

The Connection Machine handles these equations well if they are differenced explicitly. We split the Vlasov equation into the following two equations:²¹

$$\frac{\partial f}{\partial \tau} + (c - \frac{p_z}{\gamma m}) \frac{\partial f}{\partial \zeta} = 0 \quad (\text{A11})$$

and

$$\frac{\partial f}{\partial \tau} + \frac{\partial}{\partial p_z} \left[(E_z + \frac{p_x B_y}{\gamma m c} - \frac{p_y B_x}{\gamma m c}) f \right] = 0 . \quad (\text{A12})$$

For the first of these equations, we do a simple upwind differencing. For the second, we use a flux-corrected transport (FCT) algorithm.²²

References

1. T. Tajima and J. M. Dawson, Phys. Rev. Lett. 43, 267 (1979).
2. P. Chen, J. M. Dawson, R. W. Huff and T. Katsouleas, Phys. Rev. Lett. 54, 693 (1985).
3. P. Sprangle, E. Esarey, A. Ting and G. Joyce, Appl. Phys. Lett. 53, 2146 (1988); E. Esarey, A. Ting, P. Sprangle and G. Joyce, Comments Plasma Phys. Controlled Fusion 12, 191 (1989).
4. J. B. Rosenzweig, D. B. Cline, B. Cole, H. Figueroa, W. Gai, R. Konecny, J. Norem, P. Schoessow and J. Simpson, Phys. Rev. Lett. 61, 98 (1988); J. B. Rosenzweig, P. Schoessow, B. Cole, W. Gai, R. Konecny, J. Norem, and J. Simpson, Phys. Rev. A 39, 1586 (1989).
5. A. W. Chao, in Physics of High Energy Particle Accelerators: AIP Conference proceedings No. 105 (AIP, New York, 1983) p. 353.; J. T. Seeman, IEEE Trans. Nucl. Sci. 30, 3180 (1983).
6. K. L. F. Bane, P. Chen and P. B. Wilson, IEEE Trans. Nucl. Sci. 32, 3524 (1985).
7. J. B. Rosenzweig, Phys. Rev. Lett. 58, 555 (1987); IEEE Trans. Plas. Sci. 15-2, 186 (1987).
8. A. I. Akhiezer and R. V. Polovin, Soviet Physics, JETP 3, 696 (1956).
9. J. M. Dawson, Phys. Rev. 113, 383 (1959).
10. R. J. Noble, in Proceedings of the Twelfth International Conference on High Energy Accelerators, Batavia, Illinois, 1983, edited by F. Cole and R. Donaldson (Fermilab, Batavia, 1984), p. 467.
11. R. D. Ruth, A. Chao, P. L. Morton and P. B. Wilson, Part. Accel. 17, 171 (1985).
12. P. Sprangle, E. Esarey and A. Ting, Phys. Rev. Lett. 64, 2011 (1990); Phys. Rev. A 41, 4463 (1990); A. Ting, E. Esarey and P. Sprangle, Phys. Fluids B 2, 1390 (1990).
13. T. P. Coffey, Phys. Fluids 14, 1402 (1971).
14. T. Katsouleas and W. B. Mori, Phys. Rev. Lett. 61, 90 (1988).
15. J. B. Rosenzweig, Phys. Rev. A 38, 3634 (1988).
16. J. B. Rosenzweig, Phys. Rev. A 40, 5249 (1989).
17. E. Esarey, P. Sprangle and A. Ting, Bull. Am. Phys. Soc. 34, 1989 (1989).

18. See, e.g., R. C. Davidson, Theory of Nonneutral Plasmas (W. A. Benjamin, Inc., Reading, MA, 1974), p. 14.
19. S. Humphries, Jr., Principles of Charged Particle Acceleration (Wiley-Interscience, New York, 1986), pp. 426-427.
20. P. Bertrand, A. Ghizzo, T. W. Johnston, M. Shoucri, E. Fijalkow and M. R. Feix, Phys. Fluids B 2, 1028 (1990) and references w'thin.
21. C. G. Chung and G. Knorr, J. Comput. Phys. 22, 330 (1976)
22. H. L. Rowland, P. J. Palmadesso and K. Papadopoulos, Phys. Fluids 24, 832 (1981).

$\frac{L_b}{\lambda_p}$	R	R [theory]	$\frac{E_+}{E_{wb}}$	$\frac{E_+}{E_{wb}}$ [theory]
0.83	2.09	2.09	1.81	1.83
1.63	2.90	3.00	2.71	2.82
2.79	3.78	4.00	3.63	3.86

Table 1. Simulation results for the nonlinear PWFA runs. Theoretical results are from numerical solutions to Eq. (17).

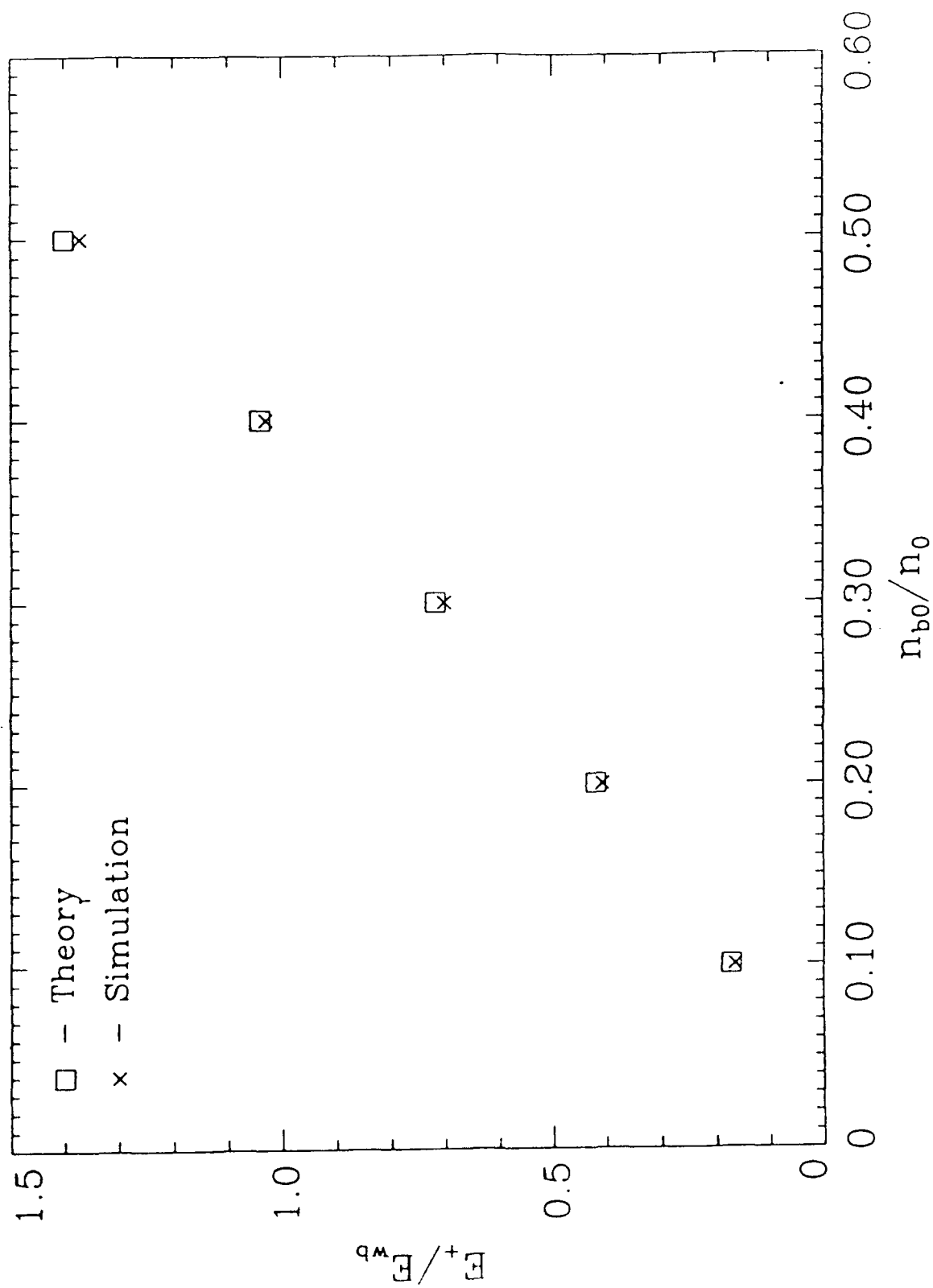


Fig. 1 Peak electric fields and corresponding theoretical values plotted versus beam density.

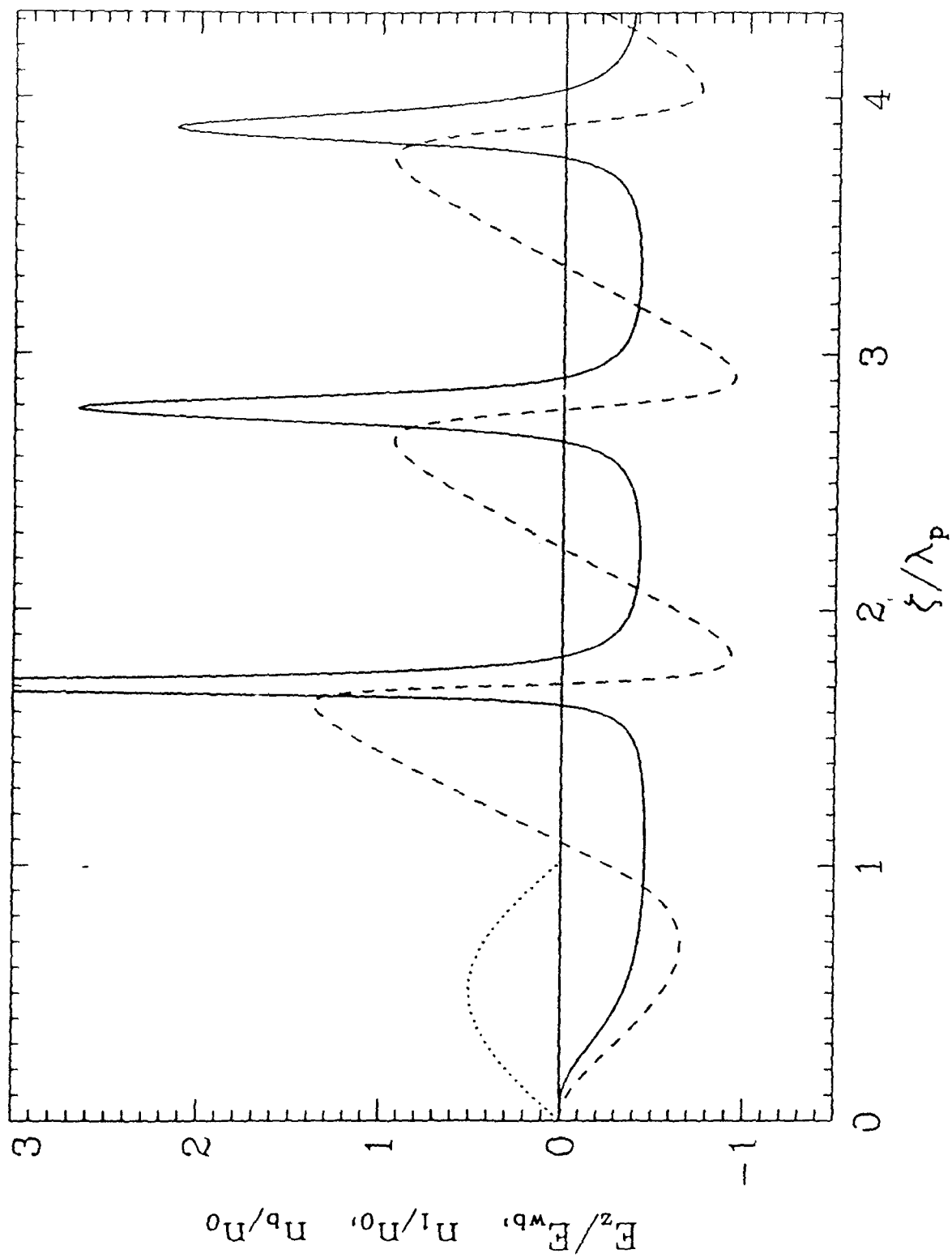


Fig. 2 Simulation result showing beam density (dotted), electric field (dashed) and perturbed plasma density (solid) plotted versus ζ at fixed time for the $n_{b0}/n_0 = 0.5$ case.

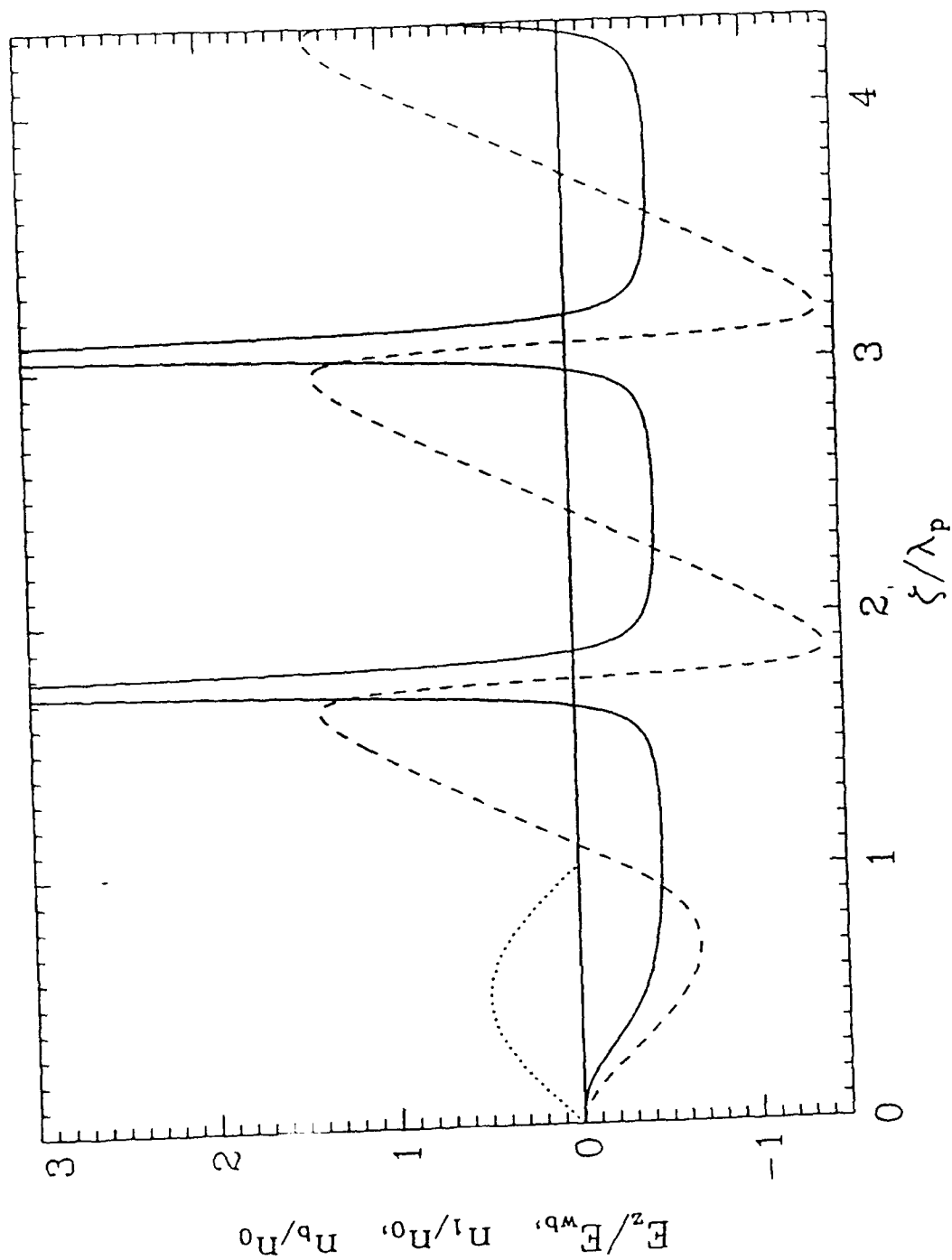


Fig. 3 Cold fluid model result for comparison to Fig. 2.

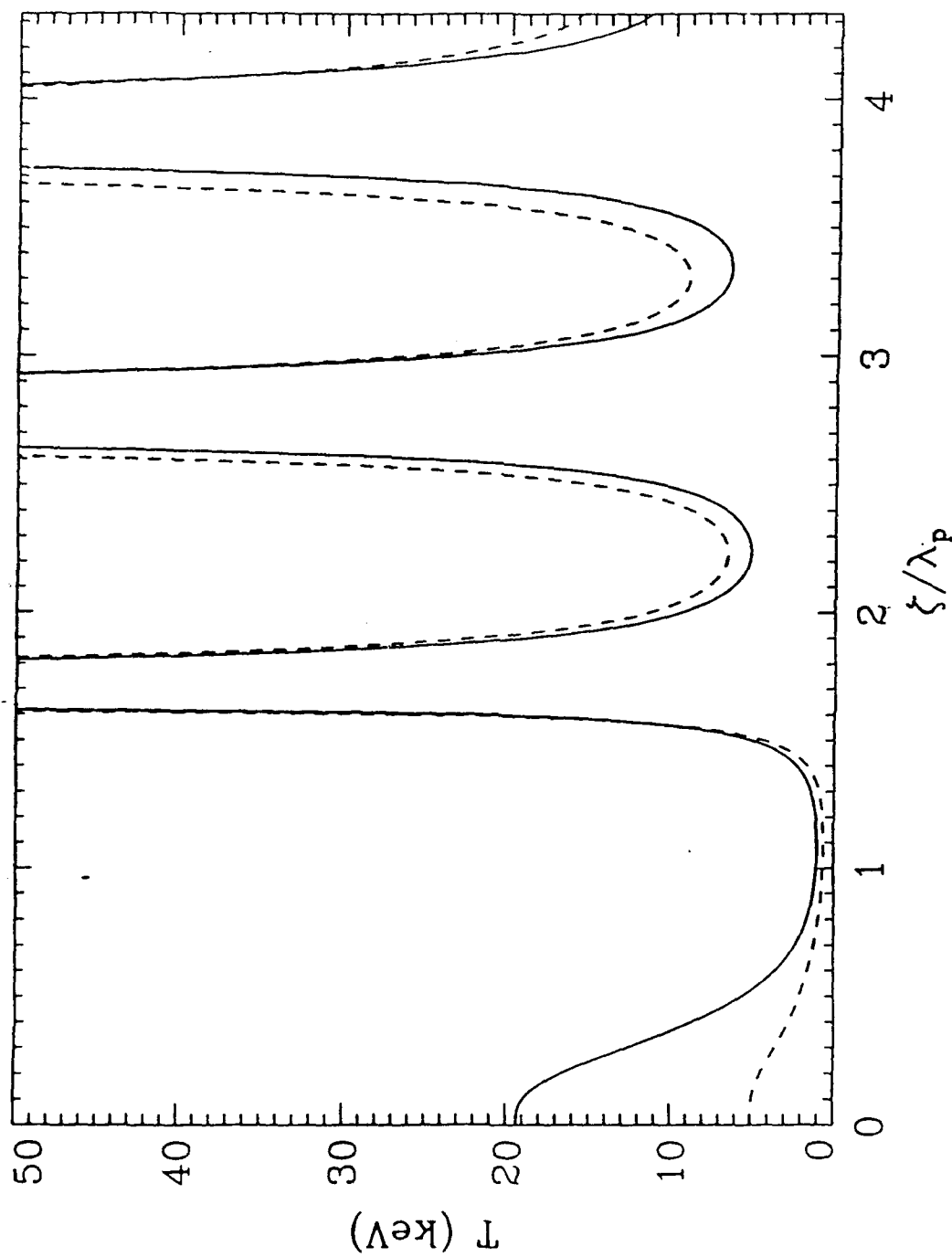


Fig. 4 Plots of temperature versus z at fixed time show insensitivity with respect to the initial temperature in the $n_{b0}/n_0 = 0.5$ case.

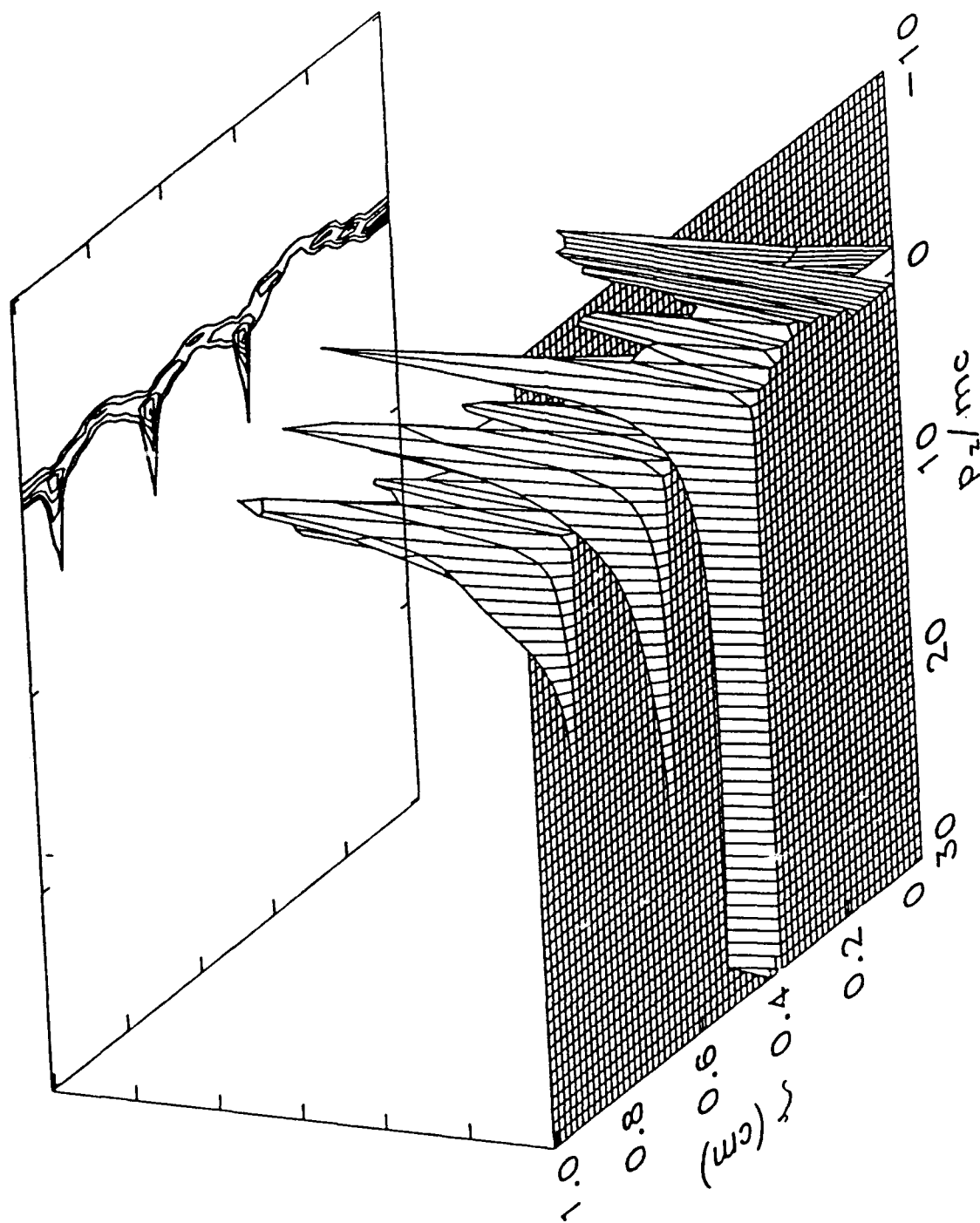


Fig. 5 The plasma electron distribution, sampled over a coarse grid, is plotted versus p_z and z at fixed time. The simulation grid is much finer.

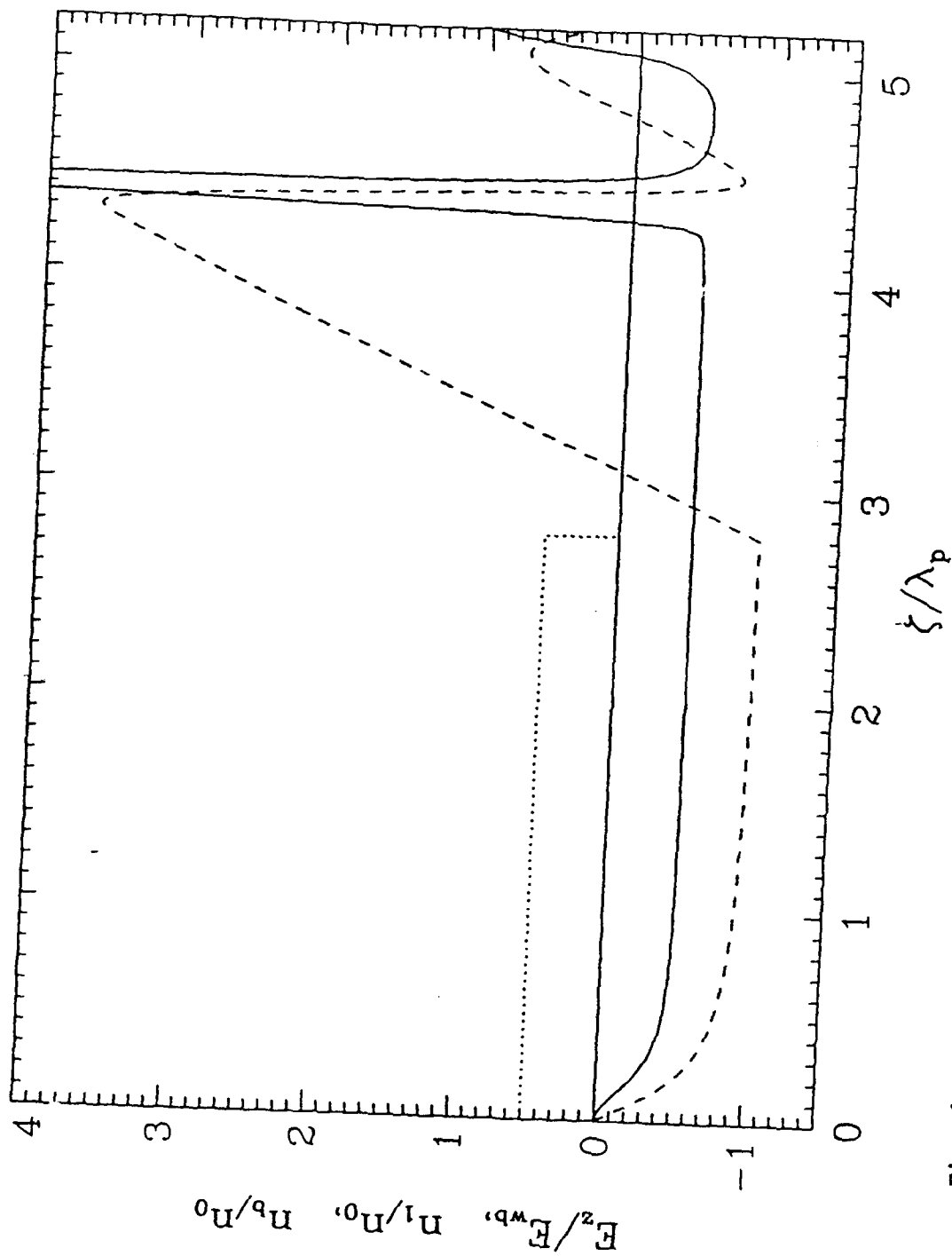


Fig. 6 Simulation result showing beam density (dotted), electric field (dashed) and perturbed plasma density (solid) plotted versus ζ at fixed time for the $L_b/\lambda_p = 2.79$ case.

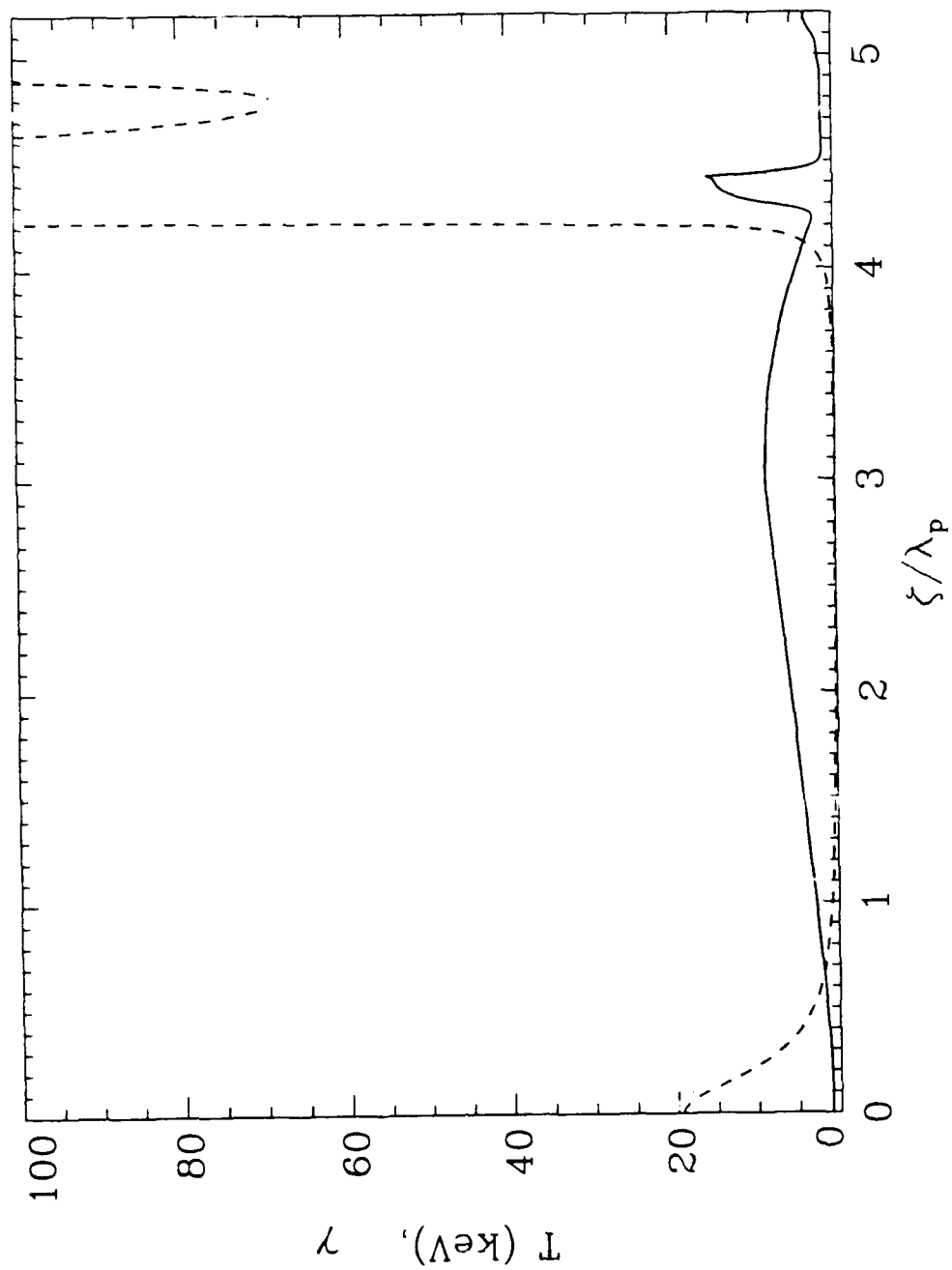


Fig. 7 Plots of temperature T (dashed) and average gamma γ (solid) for the $L_b/\lambda_p = 2.79$ case show a reduction in T as expected from Eq. (24).